Desalination and Water Treatment
www.deswater.com

doi: 10.5004/dwt.2018.21855

104 (2018) 135–148
February

Equilibrium, kinetics, mechanism and thermodynamics studies of As(III) adsorption from aqueous solution using iron impregnated used tea

Tahira Mahmood[a,*], Madeeha Aslam[a], Abdul Naeem[a], Rahmat Ali[a], Tahir Saddique[b]

[a]*National Centre of Excellence in Physical Chemistry, University of Peshawar, Peshawar, Pakistan-25120, Tel. +92919216766; Fax: +92919216671; emails: tahiramah@yahoo.com (T. Mahmood), madeeha.ncepc@gmail.com (M. Aslam), naeeem64@yahoo.com (A. Naeem), rahmatchem30@gmail.com (R. Ali)*
[b]*Department of Applied Sciences, National Textile University Faisalabad, Pakistan-37610, Tel. +923016541219; Fax: +92419230098; email: mtahir@ntu.edu.pk*

Received 8 June 2017; Accepted 22 December 2017

ABSTRACT

Considerable effort has been directed toward the removal of arsenic from an aqueous media, such as groundwater. For this purpose, used tea impregnated with iron oxide (magnetite, Fe_3O_4) particles (Fe-UT) have been tried for the removal of As(III). Different analytical techniques such as X-ray diffractometry, scanning electron microscopy/energy dispersive X-ray spectroscopy, Fourier transform infrared spectroscopy, thermogravimetric analysis (TG)/differential thermal analysis and surface area analyzer were used for the characterization of UT and Fe-UT. The average crystallite size of magnetite nanoparticles impregnated on used tea was found to be 70 nm. The removal of As(III) from aqueous solution onto the Fe-UT was carried out as a function of pH, concentration, contact time and temperature. Maximum adsorption occurred at pH 7 and 8 and then started decreasing with further increase in pH. The result of present study indicates that adsorption of As(III) on Fe-UT at pH 8 is in good agreement with WHO acceptable pH range of potable water (6.5–8.5). The adsorption capacities of the Fe-UT was substantially increased by increasing concentration while a decrease in the As(III) uptake was observed with increasing temperature of the system. The adsorption capacity for Fe-UT was found to be 3.34 mg g^{-1}. The mean free energy calculated from Dubinin–Radushkevich model confirmed the adsorption to be chemisorption and followed ligand exchange mechanism.

Keywords: As(III); Iron impregnated used tea; Ligand exchange; Isotherms; Kinetics; Thermodynamic parameters

1. Introduction

Arsenic due to its mobility and high toxicity at insignificant concentrations is considered to be the world's most hazardous contaminant and arsenic pollution has been recorded as first priority issue by World Health Organization. Arsenic enters the water both by natural (such as weathering reactions, volcanic emissions and biological activities) and anthropogenic sources (smelting of metal ores, use of arsenical insecticides, fertilizers, wood preservatives, electronics, glass and ceramic manufacturing industries) [1,2]. Arsenic exists in organic as well as inorganic forms. Toxicity of inorganic As which exists as arsenite [As(III)] and arsenate [As(V)] is more than organic form. As(III) is estimated to be 25–60 times more toxic than As(V) [3,4]. At natural pH, As(III) exists as H_3AsO_3 and $H_2AsO_3^-$ and As(V) as H_3AsO_4, $H_2AsO_4^-$, $HAsO_4^-$ and AsO_4^{3-}. As(V) is dominant and stable under oxidizing conditions in surface water, while As(III) predominates under reducing conditions in groundwater [5,6]. The most common pathway for human exposure to arsenic is through drinking water. The toxicity of arsenic is mostly due to its ability to interact with sulphydryl groups of the proteins and enzymes and thus stop the action of thiol group of enzymes [7]. As it causes toxic effects at low concentrations, the US Environmental Protection Agency has recently

* Corresponding author.

reduced the maximum contaminant limit (MCL) standard from 50 to 10 μg L^{-1}, which is also the WHO drinking water quality guideline for arsenic [5,8].

Arsenic due to its high toxicity is considered to be top of pollutant list and is carcinogenic, mutagenic and teratogenic [9]. The long-term exposure of arsenic causes cancer of liver, lungs, kidneys, skin, nasal passage and prostate. Arsenic poisoning causes neurological and endocrine disorders, diabetes, loss of appetite, muscular weakness, skin lesions, gastrointestinal and cardiovascular diseases [10–12]. Naturally occurring arsenic in drinking water threatens the health and lives of people in many countries including Canada, Chile, Japan, China, Greece, Hungary, Taiwan, Iran, Argentina, Mexico, Ghana, Vietnam, Poland, India, Bangladesh and even in Pakistan [9]. In Pakistan, drinking water of Multan, Rahimyar Khan, Jhang, Dera Ghazi Khan, Mirpur Khas, Shikarpur, Larkhana, Thatta, Dadu, Mardan and Abbottabad is badly affected by arsenic with concentration exceeding the MCL [13,14].

Arsenic removal from groundwater is a challenging task due to large variation in physiochemical forms at different conditions. Presently, numerous techniques such as ion exchange, membrane separation, precipitation–coagulation, oxidation, reverse osmosis, nanofiltration and adsorption have been proposed to remove arsenic from water [6,15]. However, the adsorption technique appears to be the most applicable because it is cost effective, easy to handle, versatile and has the ability to regenerate the adsorbent for re-use [16,17]. Considerable effort has been directed toward the removal of arsenic, for this purpose, several adsorbents such as oxides (zirconium oxide, iron oxides, manganese oxide, titanium dioxide, clay, activated alumina, mixed oxides, etc.), hydroxides (iron hydroxide, aluminium hydroxide, lanthanum hydroxide, etc.), metal phosphates (iron phosphate, etc.), agricultural and industrial wastes (rice husk, pecan nut shell, sugarcane bagasse, tea waste, hazelnut and coconut shell, peels of various fruits, calcined bauxite, red mud, etc.), polymer resins (Amberlite IRC-718, amberlite XAD-7, PolyHIPE, etc.), biosorbents (coconut shell, mango leaf, orange peel, rice polish, banana peel, etc.) and activated carbon have been tested by different researchers for the removal of arsenic from aqueous solution [10,11,18–20].

In the present study, black tea (*Camellia sinensis*) leaves are used as an adsorbent as it is the most popular and extensively consumed non-alcoholic beverage worldwide after water. Pakistan is a major tea-consuming country, annually 240,000 tons of tea are consumed in Pakistan, placing it as the seventh largest tea-consuming country in the world. It is consumed in thousands of tons every year and its proper disposal after use is a serious problem. The use of such environment friendly starting material as an adsorbent may reduce solid waste pollution and also cost of raw material for the adsorption process. Moreover, the structure of tea shows that cell walls of tea leaves are made of tannins, cellulose, lignin and hemicelluloses. These possess different functional groups such as oxyl, phenolic hydroxyl, carboxylate and aromatic carboxylate that act as metal scavengers and are responsible for adsorption of heavy metals on tea [21]. Therefore using this waste as an adsorbent will not only remove arsenic from water but also resolve the issue of waste management.

Tea waste, spent tea leaves, green tea leaves, industry tea waste or tea waste biochar have been used as an adsorbent for the removal of various contaminants such as dyes, phenols and heavy metals from aqueous solutions [22–26]. However, to increase the efficiency of tea waste as an adsorbent, pre-treatment with some chemicals such as alkalis, detergents and activation has been carried out [23,26,27]. Hence, further research on its modification is gaining importance to enhance affinity of tea waste for removal of various kinds of pollutants from waste water.

Iron oxides (either in bulk form or nanoparticles) due to their low cost, non-toxicity and higher affinity for arsenic are mostly used as an adsorbent for removal of arsenic. The application of iron oxide nanoparticles due to their large surface area and strong adsorption characteristics in contaminant remediation has enhanced the adsorption process [28,29]. Recently, magnetic (Fe_3O_4) materials have attracted special attention in water treatment due to their strong adsorption affinities and the properties of being easily separated and reused by an external magnetic field [5].

To the best of our knowledge, no former work has reported modified used tea (household) for the selective removal of arsenic As(III). The present work aims to investigate the possible use of abundantly available tea waste (UT) for the adsorption of As(III) from aqueous solution. Moreover, UT was impregnated with iron oxide (magnetite) particles to increase the adsorption capacity of As(III). The structural, morphological and spectral properties of adsorbents were investigated through different techniques. The effect of various factors such as contact time, initial metal ion concentration, pH and temperature on adsorption was systematically examined. The equilibrium study will provide information regarding the affinity between the adsorbate and adsorbent. Equilibrium and kinetic studies were carried out at different temperatures. The experimental data were fitted with different models in order to determine whether the adsorption process was physisorption or chemisorption. Additionally, several thermodynamic parameters such as the enthalpy, entropy and Gibbs free energy were calculated. Moreover, the adsorption capacity of Fe-UT was tested and compared with various other adsorbents already used for the removal of As(III).

2. Experimental design

2.1. Chemicals and reagents

Throughout the research work, all chemicals used were of analytical reagent grade and were used without further purification. All the chemicals including ferric chloride hexahydrate, ferrous sulphate heptahydrate, ammonium hydroxide, hydrochloric acid, sodium hydroxide, nitric acid and sodium nitrate were purchased from Scharlau (Spain). All the stock and working solutions were prepared in distilled deionized water. Prior to the experiment, glassware used was first washed with tap water, followed by 10% nitric acid solution and finally rinsed with deionized water. Arsenic standards for atomic absorption spectrophotometer were purchased from Scharlau Company.

2.2. Preparation of adsorbents

Used black tea (UT) of Lipton brand collected from domestic source was boiled with deionized water at 80°C for 1 h to remove its color, caffeine and tannins. It was further

washed several times with double distilled water until colorless filtrate was obtained. It was then dried in an oven at 105°C for 24 h. The dried material was crushed and sieved to 120 mesh sizes.

Modification of the used tea (UT) was carried out by impregnating with iron oxide (Fe_3O_4) fine particles. Synthesis of magnetite fine particles (Fe_3O_4) was carried out by the homogenous precipitation method reported by Panneerselvam et al. [30]. In this process, 3.1 g of $FeCl_3.6H_2O$ and 2.1 g of $FeSO_4.7H_2O$ were dissolved in 80 mL of deionized water under inert atmosphere with vigorous stirring. The solution was heated to 80°C, when the required temperature was achieved; 10 mL of NH_4OH solution (25%) was drop wise added to obtain the formation of black precipitates of Fe_3O_4 fine particles. These were then mixed with 10 g of adsorbent (UT) and heated at 80°C for half an hour under vigorous stirring. The resulting suspension was cooled down to room temperature and then washed several times with deionized water to remove impurities. The reaction involved during UT impregnation is represented by Eq. (2):

$$FeSO_4{\cdot}7H_2O + 2FeCl_3{\cdot}6H_2O + 8NH_4OH \rightarrow Fe_3O_4 + 6NH_4Cl + (NH_4)_2SO_4 + 17H_2O \quad (1)$$

$$Fe_3O_4 + UT \rightarrow UT\text{-}Fe_3O_4 \quad (2)$$

The iron oxide impregnated used tea (UT-Fe_3O_4) was dried in an oven for 24 h at 110°C and will be onwards referred to as Fe-UT.

2.3. Characterization

The prepared adsorbents (UT and Fe-UT) were characterized by using various analytical techniques. Surface area analyzer (NOVA 1200e, Quantachrome, USA) was used to determine the surface areas (S_{BET}) of the adsorbents by nitrogen adsorption/desorption method. The morphologies of adsorbents were examined by scanning electron microscopy (SEM; JSM-6490, JEOL, Japan) at 20 keV and elemental composition of the adsorbents was determined by energy dispersive X-ray analyzer (EDX Inca-200). FTIR analyses of the adsorbents were carried out in the wavelength range of 400–4,000 cm^{-1} using an infrared spectrophotometer (8201PC, Shimadzu, Japan). The X-ray diffraction patterns of the samples were recorded in the 2θ range from 10° to 80° using JEOL X-ray diffractometer (model JDX-3532) with Mn filtered Cu-Kα radiations. The batch experiments were performed by taking 40 mL of 0.1 N $NaNO_3$ solutions in 100 mL titration flasks and the initial pH (pH_i) of the solution was adjusted in the range 2–10 with either NaOH or HNO_3 solutions, using a pH meter (model BOECO BT-600 [Germany]). Afterwards, 0.1 g of adsorbent was added to each flask and shaken on a shaking bath (model WSB-30) at 298 ± 0.1 K for 24 h. After equilibration, the final pH (pH_f) of the solution was noted. The difference between the final and initial pH values (ΔpH) were plotted against the initial pH values (pH_i) to get the point of zero charge (PZC) of each of the adsorbent. Moreover, to determine the stability of Fe-UT, after equilibration the aqueous filtrates were analyzed for the release of Fe from the Fe-UT.

2.4. Adsorption studies

Batch adsorption experiments were conducted to examine the effect of concentration, pH and temperature on the adsorption of As(III) onto Fe-UT. The working solutions of As(III) were prepared from 1,000 mg L^{-1} standard solution of As(III). Detailed adsorption studies were carried out for the adsorption of As(III) onto Fe-UT to probe into the mechanism of the adsorption process. For each experiment, 0.1 g of the adsorbent was added to 40 mL of As(III) solution of different concentrations (5–100 mg L^{-1}). The initial pH of each solution was adjusted to 8 using either hydrochloric acid or sodium hydroxide solution. The samples were placed in shaker at a shaking speed of 120 rpm at 298 K for 24 h. After equilibration, the final pH of each solution was noted. All the solutions were then filtered and the filtrates were analyzed for As(III) and iron released from the iron impregnated used tea using atomic absorption spectrophotometer (AAS 800). The amount of As(III) adsorbed (X) was determined from the difference of the initial and the equilibrium concentration of the As(III) in aqueous solution by using the following expression:

$$X = \frac{V(C_i - C_e)}{1000m} \quad (3)$$

where V refers to the volume of the solution (mL), m is the mass of the adsorbent (g), and C_i and C_e are the initial and equilibrium concentrations (mol L^{-1}) of As(III), respectively.

Adsorption studies of arsenite onto UT were also conducted for comparison with Fe-UT at pH 8 and 298 K. The effect of pH was examined at various pH values (3–12) at 298 K with different concentrations of As(III) solutions for the removal of As(III) by Fe-UT. Temperature studies were carried out at 298–328 K at pH 8 with different concentrations of As(III) solutions. Adsorption kinetics experiments for 25 mg L^{-1}As(III) were carried out at pH 8 at different temperatures (298–318 K) and various time intervals (5 min to 24 h). Adsorption studies of arsenite onto UT were also conducted for comparison with Fe-UT at pH 8 and 298 K.

3. Results and discussion

3.1. Characterization

3.1.1. Surface area and pore size distribution

The Brunauer–Emmett–Teller (BET) surface areas of UT and Fe-UT are given in Table 1. The BET surface area for the UT and Fe-UT was 80 and 66 m^2 g^{-1}. This decrease in surface area can be attributed to the covering of UT surface by iron oxide particles during impregnation which was also confirmed later by the SEM results. These iron particles have small surface area and microporous volume, which block the pores of the adsorbent surface and thus results in the reduction of surface area and pore size [31]. Decrease in surface area was also observed by Liu et al. [32] while impregnating bamboo charcoal with iron oxide.

The pore diameter and pore volume of UT were found to be 118 Å and 1.68 cc g^{-1}, respectively. These values decrease to 76 Å and 0.11 cc g^{-1} for Fe-UT. The average pore diameters of all the adsorbents lie in the range of 20–500 Å. This pore size distribution suggests that the adsorbents used in

Table 1
Surface area, pore size distribution and elemental composition of UT and Fe-UT

Adsorbent	UT	Fe-UT
Surface area ($m^2\ g^{-1}$)	80	66
Pore diameter (Å)	118.5	75.69
Pore volume (cc g^{-1})	1.68	0.11
Elemental composition % weight		
C	63	33
O	12.8	29
B	23	–
Ca	1.2	1
Fe	–	37

this study are mesoporous in nature according to the pore classification of the International Union of Pure and Applied Chemistry [33].

3.1.2. SEM/EDX and FTIR analysis

The SEM images (Figs. 1(a)–(c)) helps to observe the surface morphology of adsorbents on micron levels and it is widely used to observe the arrangement of particles on the surface of adsorbents. In the present study, the SEM image (Fig. 1(a)) illustrates an irregular shape of UT with heterogeneous pores. The porous nature of UT suggests the availability of more surface area for adsorption of molecules. The decrease in porosity in the case of Fe-UT was observed as compared with its precursor UT (Fig. 1(b)) which is most

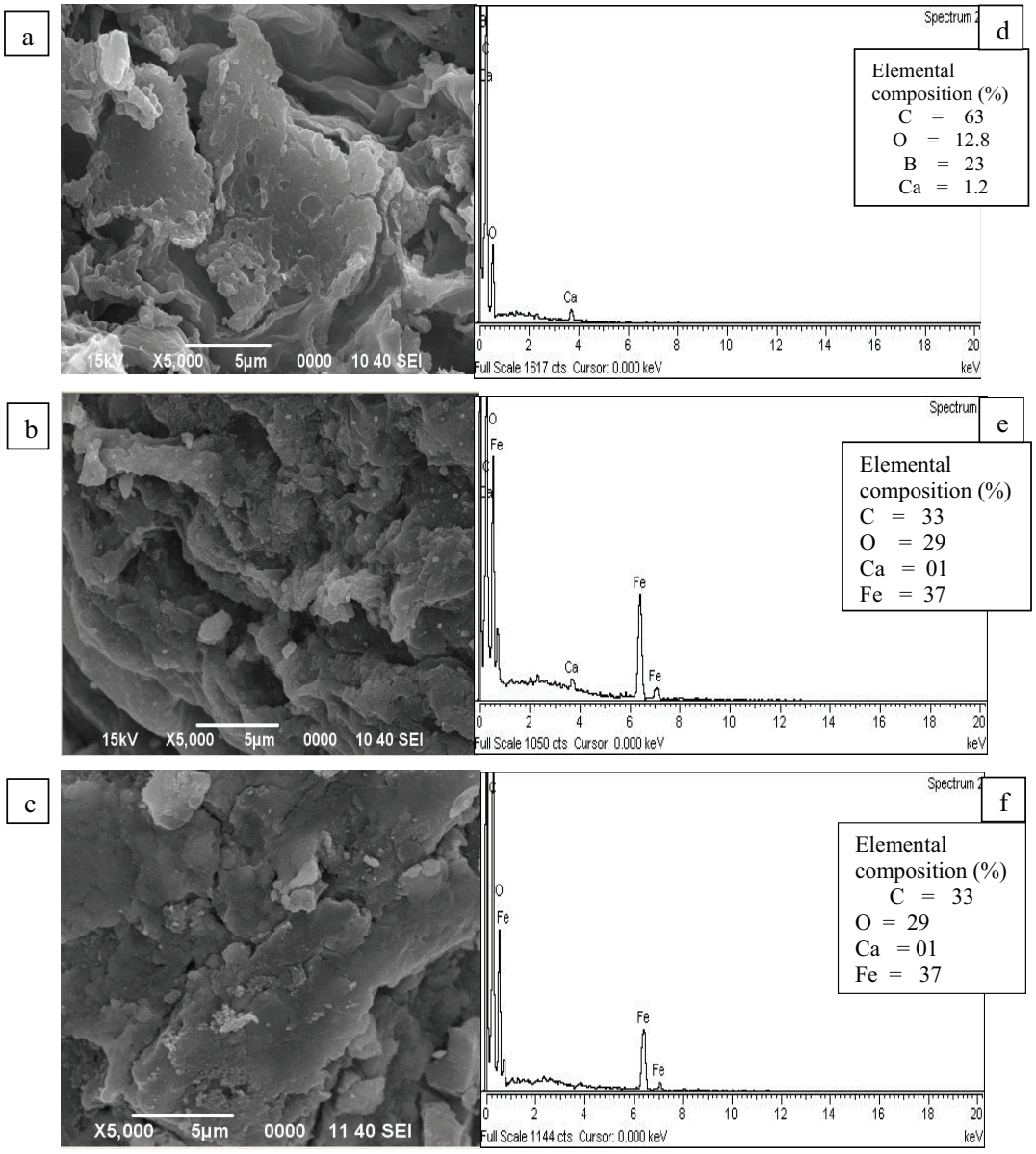

Fig. 1. SEM/EDX images of (a) UT, (b) Fe-UT and (c) Fe-UT after adsorption.

probably due to the blockage of pores of UT by iron oxide particles [34]. Thus, it is suggested that impregnation of UT by iron oxide has been done effectively. SEM image of Fe-UT after adsorption (Fig. 1(c)) shows an obvious change in morphology, indicating that arsenic was adsorbed on Fe-UT. Irem et al. [13] also reported changes in morphology of orange waste after arsenic adsorption.

Energy dispersive X-ray spectroscopy (EDX) was used for elemental analysis of the samples. EDX patterns are shown in Figs. 1(d)–(f) and data in Table 1. EDX data of UT showed weight % composition of carbon, boron, oxygen and calcium to be 63%, 23%, 12.8% and 1.2%, respectively. While Fe-UT consists of carbon (33%), oxygen (29%), calcium (1%) and iron (37%). EDX of Fe-UT signified a considerable amount of Fe in the sample, thus suggesting the presence of iron in Fe-UT which strongly supports the impregnation of UT with iron oxide. However, no arsenic peak was observed in the EDX spectrum of Fe-UT after As(III) adsorption, due to low concentration of arsenic adsorbed.

The IR spectra of UT and Fe-UT are given in Fig. 2. The IR spectrum of UT (Fig. 2(a)) shows a number of absorption peaks, signifying the intricate nature of adsorbent. A broad band was observed at 3,392 cm^{-1}, which was assigned to –OH group, while the weak bands observed at about 2,980 and 2,180 cm^{-1} were ascribed to the C–H stretching [13]. The peak observed at 1,691 cm^{-1} was due to C=O stretching, while the small peak appeared at 1,100 cm^{-1} could be assigned to $–SO_3$ and –C–O stretching of the ether group, respectively, as reported by Zuorro et al. [26] for spent tea leaves. The spectra of UT and Fe-UT are almost similar. Furthermore, the appearance of a new band at 581 cm^{-1} in the case of Fe-UT (Fig. 2(b)) was assigned to the stretching and torsional vibration of Fe–O. The appearance of a band at ~580–620 cm^{-1} corresponding to Fe–O stretching confirmed the loading of Fe oxide onto UT [35]. Similarly, Karaagac et al. [36] observed a broad band at 560–580 cm^{-1} which was associated with the vibrations of Fe–O bond.

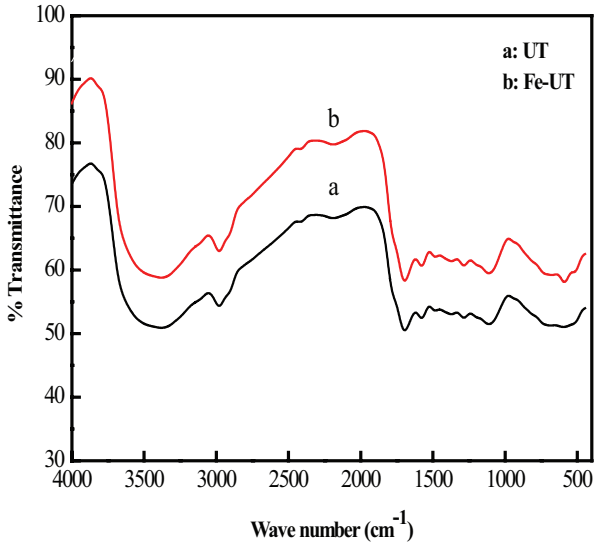

Fig. 2. FTIR spectra of (a) UT and (b) Fe-UT.

3.1.3. XRD and thermogravimetric analysis

The XRD spectra of UT (Fig. 3(a)) indicated their amorphous nature. However, the XRD pattern of Fe-UT (Fig. 3(b)) showed that it is crystalline, having peaks at 2θ (30.2°, 35.5°, 43.1°, 53.6°, 57° and 62.7°) which are the characteristic peaks of inverse-spinel structure of Fe_3O_4 matching with the international centre for diffraction data (card No. 110614). This indicated that impregnation with iron oxide has been done effectively resulting in crystalline Fe-UT, consistent with those reported elsewhere [34,37]. The crystallite size was calculated using the Debye-Scherrer equation:

$$d = \frac{k\lambda}{\beta\cos\theta} \quad (4)$$

where k is the Debye-Scherrer constant (0.89), β is the full width at half maximum, λ is the wavelength (1.54 Å) and θ is the Bragg's angle. The average crystallite size of the three intense peaks at 2θ (35.5°, 57° and 62°) was found to be 70 nm.

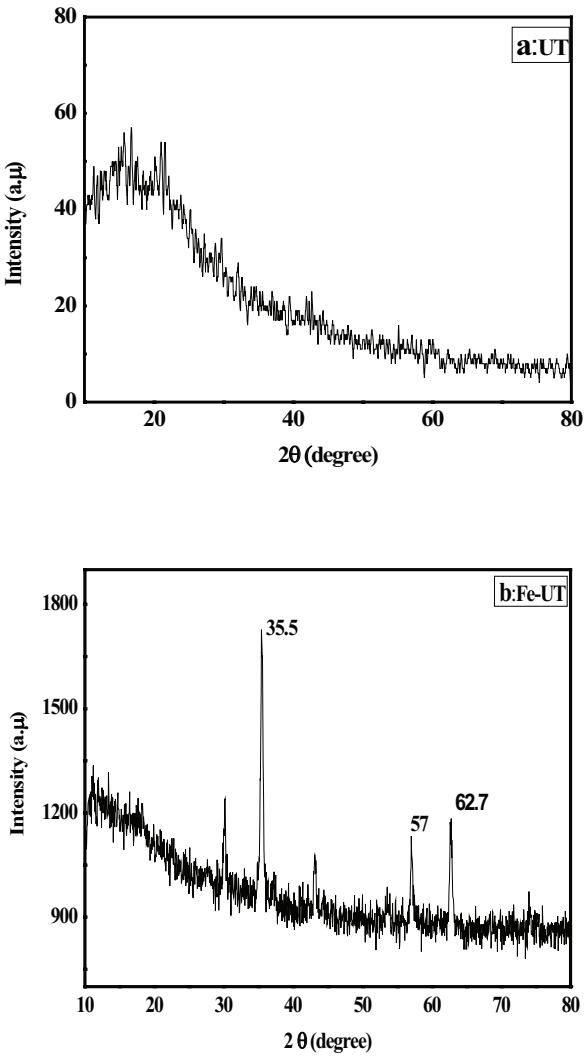

Fig. 3. XRD patterns of (a) UT and (b) Fe-UT.

Thermogravimetric analysis (TGA) and differential thermal analysis (DTA) of Fe-UT was carried out up to 1,000°C. The TG and DTA curves of Fe-UT are shown in Fig. 4(a). There was a small amount of weight loss (4.78%) below 100°C which is attributed to desorption of the physisorbed water. In the second step, the TGA curve showed a weight loss of 7.72% up to 240°C, which may be due to the pyrolysis of organic matter and some light gases such as CO_2 and CO and volatile components may also be released as reported by Mahmood et al. [38]. The third step showed the gradual weight loss of 40.3% at 380°C, which may be due to the thermal decomposition of cellulose, hemicelluloses and lignin as reported by Yagmur et al. [39] which is also evident from the exothermic DTA peaks observed in this temperature range. The fourth weight loss of 35.7% was calculated in the temperature range of 380°C–900°C which may be due to degradation of lignin. Beyond this temperature, the weight loss of Fe-UT gradually slows down and then becomes stable.

3.1.4. Point of zero charge

The point of zero charge is an important property and is defined as the pH where the net surface charges are zero, that is, it indicates the electrical neutrality of the adsorbent and the surface. The plots of ΔpH vs. pH_i yield the PZC at a pH where ΔpH is zero. The PZC of the UT and Fe-UT was observed to be at pH 6.0 and 6.30 ± 0.1 and are shown in Fig. 4(b). The PZC of Fe-UT was found to be slightly higher than UT. The PZC values are in agreement to ones reported in the literature [30,40].

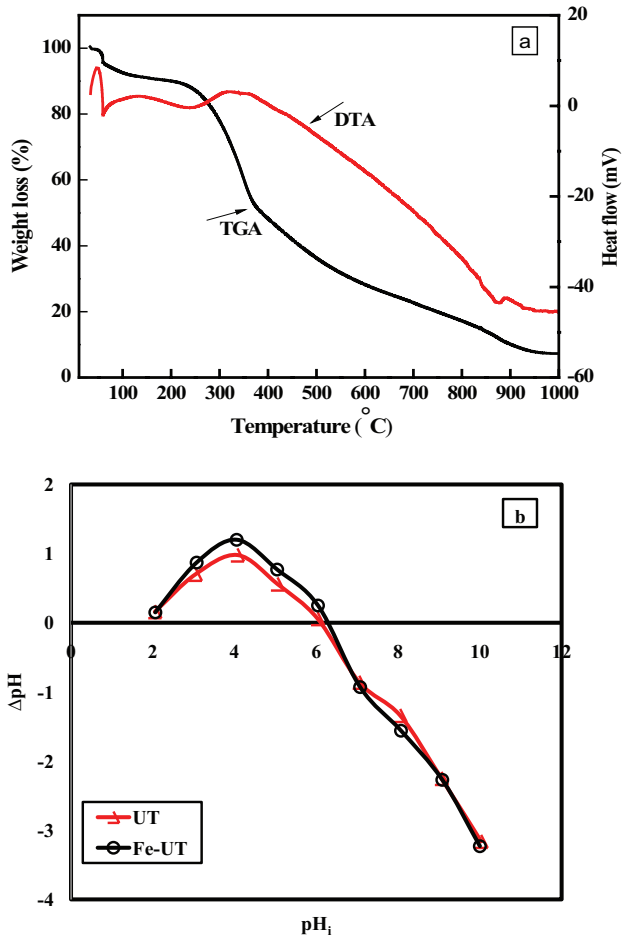

Fig. 4. (a) TG/DTA curve and (b) PZC plot of Fe-UT.

3.2. Adsorption kinetics

The kinetics of As(III) adsorption onto Fe-UT was studied to investigate the adsorption behavior of the system. The adsorption of As(III) on Fe-UT at different time intervals (5 min – 24 h) and pH 8 is shown in Fig. 5(a). The figure shows a rapid uptake of As(III) in the first 240 min, followed by a steady and slower uptake until an equilibrium is attained in 360 min. The rapid uptake of As(III) in the beginning can be attributed to the presence of a large number of vacant sites on the surface of Fe-UT. However, the adsorbent surface gets saturated after certain time period, equilibrium is established in the system and no further adsorption of As(III) occurs. Similar equilibrium time for As(III) adsorption by α-Fe_2O_3 impregnated chitosan beads has been reported by Liu et al. [41]. It is obvious from the figure that the adsorption curves of arsenite are smooth and continuous leading to saturation, suggesting the probability of monolayer coverage of the surface.

Temperature has a significant effect on the kinetics of arsenite adsorption onto Fe-UT, and the uptake of arsenite decreases with the rise of temperature from 298–318 K (Fig. 5(a)). The decrease in arsenite adsorption with increase in temperature indicates that the adsorption process is exothermic. However, the equilibrium time for the arsenite adsorption remained the same with an increase in temperature and thus is independent of temperature. Similar behavior of arsenite adsorption has been reported by Ranjan et al. [42].

3.3. Kinetic modeling

In order to explain the kinetics mechanism for the As(III) adsorption on Fe-UT, different kinetics models such as pseudo-first order, pseudo-second order, Elovich, Weber and Morris, and Richenberg models were applied to the current data.

3.3.1. Pseudo-first order and pseudo-second order model

The linear form of pseudo-first order kinetic model is given as:

$$\ln(X_e - X_t) = ln\ X_e - k_1 t \tag{5}$$

where X_t is the amount adsorbed at time t, X_e is the amount adsorbed at equilibrium time and k_1 is the rate constant. By plotting ln $(X_e - X_t)$ vs. t, straight lines were obtained and are shown in Fig. 5(b). The amount adsorbed (X_e) and rate constant (k_1) were calculated from intercepts and slopes of the plots and are summarized in Table 2. The pseudo-first order model failed to explain the current data due to the poor R^2 values and difference between experimental and theoretical values. Similar results have been reported by Mahmood et al. [43] for arsenate adsorption onto iron hydroxide.

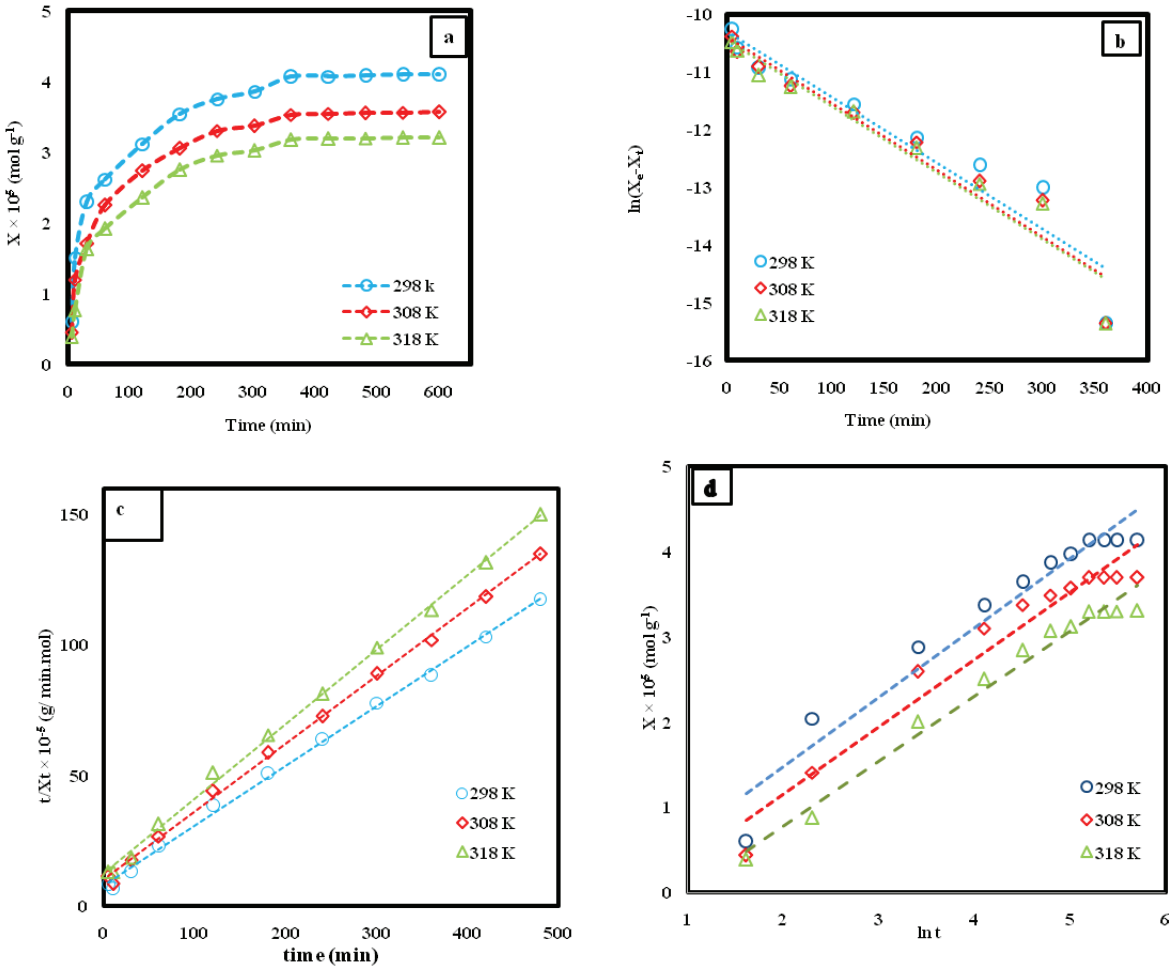

Fig. 5. (a) Effect of contact time, Plots of (b) Pseudo first order, (c) Pseudo second order and (d) Elovich model for As(III) adsorption onto Fe-UT at pH 8.

The pseudo-second order kinetic model in its linear form is given as:

$$\frac{t}{X_t} = \frac{1}{k_2 X_e^2} + \frac{1}{X_e} t \tag{6}$$

where X_e and X_t are the amount of arsenite adsorbed at equilibrium and at time t, respectively, and k_2 is the pseudo-second order rate constant. A straight line was obtained from the plot of t/X_t vs. t with $R^2 > 0.99$ (Fig. 5(c)). The values of rate constant (k_2) and amount adsorbed (X_e) were calculated from intercept and slope, respectively (Table 2). The amount of As(III) adsorbed (X_e) calculated theoretically from the pseudo-second order model is comparable in magnitude with its experimental value. This suggests that the current experimental data follow the pseudo-second order model. A similar decrease in the rate constant values with increase in temperature has been reported by Ranjan et al. [42] for biosorption of arsenite using agricultural residue rice polish.

Both the k_2 and X_e values decrease with increase in temperature, which indicates the exothermic nature of the process. The application of the pseudo-second order equation suggests that chemisorption is the possible route of As(III) adsorption onto Fe-UT.

3.3.2. Elovich model

The Elovich equation can be written in the following form:

$$X = \frac{\ln(\alpha\beta)}{\beta} + \frac{lnt}{\beta} \tag{7}$$

where α and β are constants representing the rate of chemisorption at zero coverage and the extent of surface coverage and activation energy for chemisorption. These constants were calculated from the intercept and slope of the plots of X vs. ln t (Fig. 5(d)) which showed good linear relationships with R^2 values greater than 0.9 at all temperatures and are represented in Table 3. This suggests that the adsorption of As(III) onto Fe-UT followed the pseudo-second order kinetic model based on the assumption that chemisorption may be the rate determining step.

Table 2
Pseudo first and second order parameters for As(III) adsorption onto Fe-UT at pH 8 and different temperatures

Pseudo-first order					Pseudo-second order		
Temperature (K)	Experimental $X_e \times 10^5$ (mol g^{-1})	Theoretical $X_e \times 10^5$ (mol g^{-1})	$k_1 \times 10^3$ (min^{-1})	R^2	Theoretical $X_e \times 10^5$ (mol g^{-1})	$k_2 \times 10^{-3}$ (g min^{-1}mol^{-1})	R^2
298	4.08	3.73	12.5	0.93	4.36	0.69	0.99
308	3.55	3.35	12.5	0.95	3.83	0.68	0.99
318	3.19	2.89	11.5	0.93	3.49	0.66	0.99

Table 3
Weber Morris and Elovich model parameters for As(III) adsorption onto Fe-UT at pH 8 and different temperatures

Weber–Morris model				Elovich model		
Temperature (K)	$K_{id} \times 10^6$ (mol g^{-1} min$^{-0.5}$)	C	R^2	$\beta \times 10^5$ (g mol^{-1})	$\alpha \times 10^{-5}$ (mol g^{-1} min^{-1})	R^2
298	1.96	1.34	0.78	0.82	1.04	0.94
308	1.90	1.04	0.77	0.78	0.74	0.95
318	1.88	0.62	0.85	0.76	0.49	0.98

3.3.3. Weber and Morris model

The Weber–Morris model was applied to the kinetic data to explore the possibility of intraparticle diffusion as the rate limiting step. It is an empirical equation and can be mathematically written as:

$$X = k_{id} t^{0.5} + C \tag{8}$$

where C is the intercept, a constant representing boundary layer effect and K_{id} (mol g^{-1} min$^{-0.5}$) is the intraparticle diffusion rate constant obtained from the slope of plots of X vs. $t^{0.5}$ (Fig. 6(a)). The values of K_{id} at different temperatures are given in Table 3.

The larger the value of C, the greater is the boundary layer effect. If the plot of X vs. $t^{0.5}$ is linear and passes through the origin with no intercept, intraparticle diffusion is the rate determining step. In the present study, linear plots of X vs. $t^{0.5}$ do not pass through the origin, which means that intraparticle diffusion is not the only rate determining step. The adsorption process may be controlled by more than one mechanism with the initial curved portions of the plots (Fig. 6(a)) suggesting film diffusion (boundary layer) and the linear portions representing intraparticle diffusion. The present findings are in agreement with the data reported in literature [32].

3.3.4. Richenberg model

The Richenberg model which differentiates between film and intraparticle diffusion is given as follows:

$$F = 1 - \frac{6}{\pi^2} \sum_m^1 \frac{1}{m^2} \exp(-m^2 B_t) \tag{9}$$

where F is the fractional attainment of equilibrium at time t, and is obtained by the following expression:

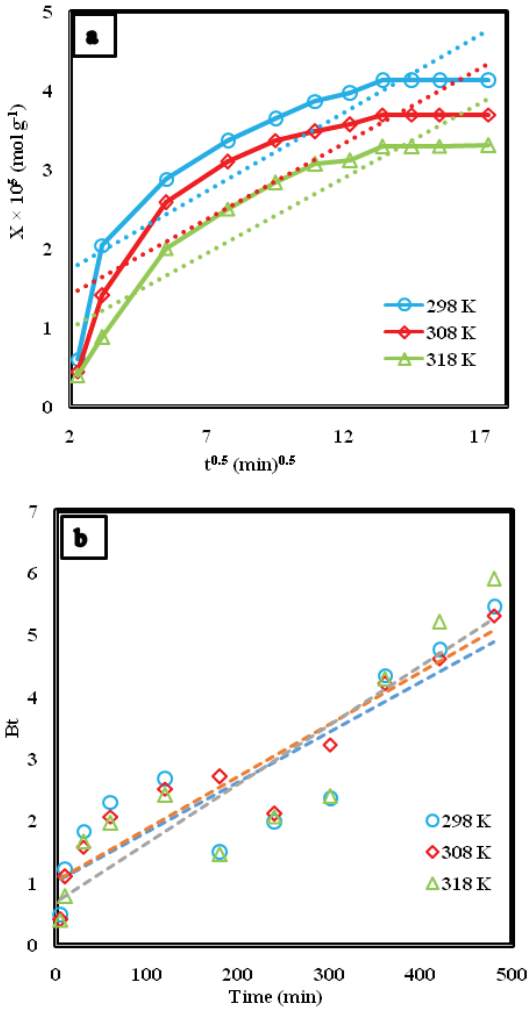

Fig. 6. (a) Weber Morris and (b) Richenberg plots for As(III) adsorption onto Fe-UT.

$$F = \frac{X_t}{X_e} \tag{10}$$

B_t is a mathematical function of X which can be evaluated from the equation given below:

F values < 0.85

$$B_t = -0.4977 - \ln(1 - F) \tag{11}$$

and for

F values > 0.85

$$B_t = (\sqrt{\pi} - \sqrt{\pi - \frac{\pi^2 F}{3}})^2 \tag{12}$$

The plots of B_t vs. t at different temperatures are shown in Fig. 6(b). If a plot of B_t vs. t is linear passing through the origin, then the rate determining step is particle diffusion, otherwise, it is followed by film diffusion. In the present study, the plots are straight lines, but do not pass through the origin. Hence, it is concluded that film diffusion is the main rate limiting step for the adsorption of arsenite by Fe-UT.

3.4. Equilibrium adsorption studies

3.4.1. Effect of arsenite concentration and temperature

The effect of arsenite concentration on its adsorption onto UT and Fe-UT at 298 K is given in Fig. 7(a). An increase in arsenite concentration led to increase in the adsorption capacities (mol g^{-1}) which may be due to the availability of more arsenite ions in solution. The probability of collision between arsenite ions and adsorbent increases, which results in the increased adsorption. Arsenite adsorption by Fe-UT (4.46×10^{-5} mol g^{-1}) is almost three times greater than UT (1.43×10^{-5} mol g^{-1}). The higher adsorption capacity of Fe-UT as compared with UT can be attributed to the higher affinity of iron oxide for As(III).

Arsenite adsorption onto Fe-UT was studied at 298–328 K. It is obvious from Fig. 7(b) that temperature has a significant effect on the As(III) adsorption by Fe-UT. The uptake of arsenite onto Fe-UT was found to be maximum at 298 K and minimum at 328 K. The decrease in adsorption of arsenite onto Fe-UT indicates that the adsorption phenomenon is exothermic in nature. By increasing temperature, the attractive forces between adsorbent surface and metal ions are weakened and therefore adsorption decreases. Similar temperature effect has been reported by others [44,45].

3.4.2. Effect of pH

The pH is usually an essential factor affecting the adsorption process as it influences the surface charge of the adsorbent. The pH studies for As(III) adsorption onto Fe-UT were carried out in the range 3–12 at 298 K (Fig. 8(a)). The pH has a little effect on As(III) adsorption and maximum adsorption is observed at pH 7 and 8 that is in good agreement with a WHO acceptable pH range of potable water (6.5–8.5).

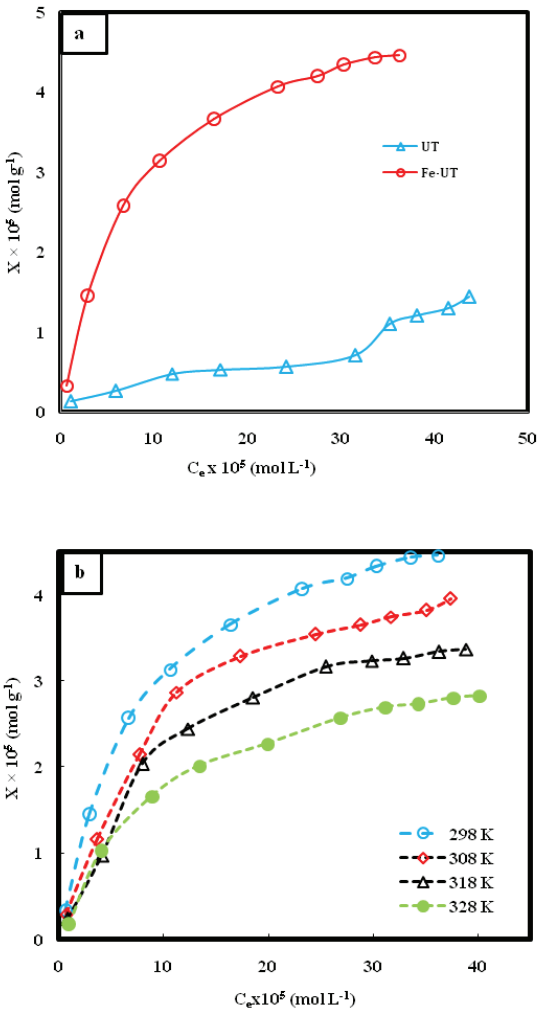

Fig. 7. (a) Effect of As(III) concentration onto UT and Fe-UT and (b) Effect of temperature on As(III) adsorption onto Fe-UT at pH 8.

Keeping in view the normal pH range of potable water, pH 8 was selected for further studies. This adsorption behavior of arsenite at different pH may be due to different oxyanionic forms of As(III). As, As(III) exists in non-ionic (H_3AsO_3) form below pH 7 and weak van der Waals forces most probably exist between H_3AsO_3 and the surface of adsorbent. But as the pH approaches 7, a small percentage of H_3AsO_3 dissociates into anionic species ($H_2AsO_3^-$ and $HAsO_3^{2-}$) and higher arsenic uptake by adsorbent (Fe-UT) is expected due to more specific binding [46]. Maximum adsorption for As(III) at pH 8 has been reported by Bibi et al. [8] for potato peel and rice husk, Vieira et al. [47] for iron-coated seaweeds and Kocabas and Yurum [48] for ferric ion loaded red mud. However, further increase in pH adsorption decreases. The decrease in As(III) adsorption at pH 9–12 may be due to the electrostatic repulsions between $H_2AsO_3^-$ and $HAsO_3^{2-}$ and the negatively charged surface. Another reason for reduced adsorption may be the competition between hydroxyl ions and arsenite anions for the same sites on the adsorbent surface [32,49]. Usually, the pH increase (beyond the pH PZC of an adsorbent, in this case 6.3) causes a lower adsorption of negative adsorbates,

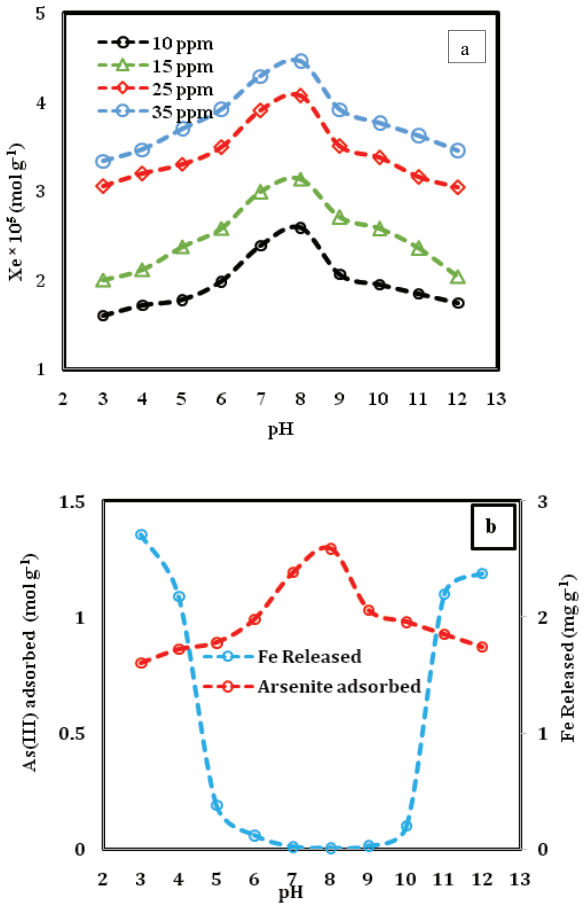

Fig. 8. (a) pH effect on arsenite adsorption onto Fe-UT (b) Release of iron from Fe-UT and As(III) adsorption at different pH.

due to the creation of a negative charge on the solid surface. This type of pattern has not been observed here for As(III). This means that the electrostatic attraction is not the predominant As(III) uptake mechanism and specific adsorption on iron sites is based on the formation of monodentate and bidentate species.

3.4.3. Mechanism of arsenic adsorption on Fe-UT

It is suggested that Fe(III) is adsorbed on UT by releasing protons from the cellulose unit according to a cation exchange mechanism. Treatment with iron results in the production of adsorption sites of magnetite particles on the exterior surface of adsorbent. The adsorbed iron will coordinate with hydroxyl ions and neutral water molecules that are available in the aqueous medium. The adsorption of arsenite on Fe-UT may be termed as a ligand exchange mechanism. Ligands involved in such exchange processes may be hydroxyl ions or neutral water molecules existing in the Fe-coordinated sphere. Thus, the adsorption of arsenite may take place by releasing a hydroxyl anion or neutral water molecules from its coordinated sphere and hence the following mechanism may be responsible for the adsorption of arsenite anions:

$$\equiv \mathrm{FeOH} + \mathrm{H_3AsO_3} \rightarrow \equiv \mathrm{FeH_2AsO_3} + \mathrm{H_2O} \quad (13)$$

$$\equiv 2\left[\mathrm{FeOH}\right] + \mathrm{H_3AsO_3} \rightarrow \equiv \mathrm{FeHAsO_3Fe} + 2\mathrm{H_2O} \quad (14)$$

$$\equiv \mathrm{FeOH} + \mathrm{H_2AsO_3^-} \rightarrow \equiv \mathrm{FeHAsO_3^-} + \mathrm{H_2O} \quad (15)$$

$$\equiv 2\left[\mathrm{FeOH}\right] + \mathrm{H_2AsO_3^-} \rightarrow \equiv \mathrm{FeHAsO_3Fe} + 2\mathrm{HO^-} + \mathrm{H^+} \quad (16)$$

where ≡ FeOH refers to the solid surface of Fe-UT. Eqs. (13) and (15) represent adsorption of arsenite on the surface of Fe-UT through monodentate ligand exchange and Eqs. (14) and (16) represent bidentate ligand exchange with hydroxyl groups.

As(III) removal at pH > 7 is due to the contribution of monovalent arsenite anion whose distribution is significant at this pH (Eqs. (13) and (14)). Whereas arsenite adsorption taking place at pH < 7 is due to the adsorption of neutral arsenite molecules accompanied by the release of water molecules according to the reaction mechanism (Eqs. (15) and (16)).

This mechanism is confirmed by its high value of free energy (E), that is, 10 kJ mol^{-1} obtained from Dubinin–Radushkevich (D–R) isotherm that showed reaction is chemisorption in nature. The mechanism is further augmented by the fact that the pH of the solution had increased or almost no change had taken place after arsenic adsorption. Similar mechanism has also been suggested by Vieira et al. [47] for arsenic removal by iron coated sea weed and Biswas et al. [50] for the removal of As(III) using Zr(IV) loaded orange waste.

It is important to mention here that no release of Fe from Fe-UT was detected in the pH range 2–12 in the absence of As(III). However, in the presence of arsenite, a slight release of iron atoms from the Fe-UT was observed (Fig. 8(b)) in the pH range 2–3 and 10–12. The release of iron in the presence of As(III) indicates that the arsenite anion is dragging iron from the Fe-UT to form complexes in the aqueous phase. The maximum arsenite adsorption in the pH range 7–8 may, therefore, also be correlated with the stability of Fe-UT as no release of iron from Fe-UT was observed in this pH range.

3.5. Adsorption models

3.5.1. Langmuir model

The Langmuir model provides useful information regarding the maximum adsorption capacity in the form of monolayer coverage. The linear form of the conventional Langmuir equation may be written as follows:

$$\frac{C_e}{X} = \frac{1}{K_b X_m} + \frac{C_e}{X_m} \quad (17)$$

where C_e and X are the amounts of arsenic in solution and at the solid surface, respectively. The values of maximum adsorption capacity (X_m) obtained from Langmuir isotherms (Fig. 9(a)) are comparable with the experimental values (Table 4). The values of binding energy constant (K_b) are

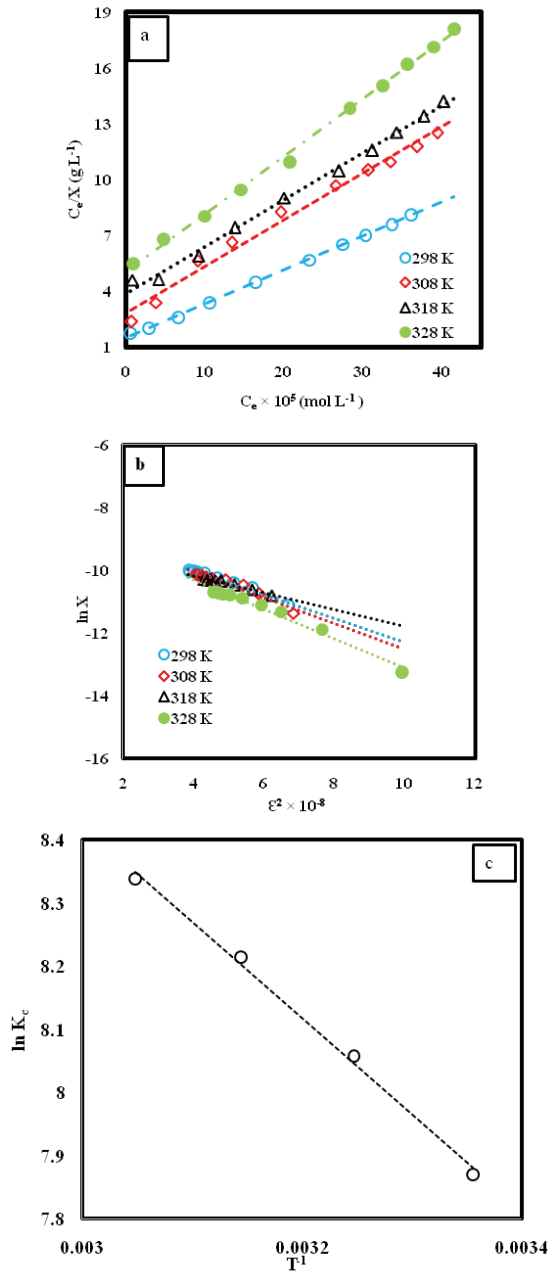

Fig. 9. Plots of (a) Langmuir model, (b) D-R model and (c) Van't Hoff for adsorption of As(III) onto Fe-UT.

sufficiently high, indicating that strong binding forces are involved in the adsorption of arsenite onto Fe-UT. The values of X_m and K_b decrease with the rise of temperature (298–328 K), which indicate that the process of adsorption is exothermic in nature. This further augments the observation made in the adsorption isotherm (Fig. 9(a)) where the adsorption was found to decrease with increase in temperature. Similar decreasing trend for X_m and K_b values with increase in temperature was reported by Ranjan et al. [42].

The feasibility of the adsorption can be predicted in terms of dimensionless constant (R_L), defined by the following expression

$$R_L = \frac{1}{1 + K_b C_i} \tag{18}$$

where K_b is the Langmuir binding constant and C_i is the initial concentration of arsenite.

$R_L > 1$ unfavorable, $R_L = 0$ irreversible, $R_L = 1$ linear, $0 < R_L < 1$ favorable [14].

The R_L values for As(III) adsorption onto Fe-UT are lesser than unity and greater than zero at all temperatures and concentrations (Table 5), suggesting favorable adsorption process. The R_L values decrease with increase in concentration of As(III) but increase with rise in temperature indicating that As(III) adsorption onto Fe-UT is more favorable at higher concentrations and lower temperature.

3.5.2. Dubinin–Radushkevich model

The D–R model which is used to determine the energy of adsorption as well as to differentiate between chemisorption and physisorption is given in its linear form as:

$$\ln X = \ln X_m - K\varepsilon^2 \tag{19}$$

where X_m (molg^{-1}) is a D–R adsorption capacity and is given as follows:

$$\varepsilon = RT \ln\left[1 + \left(\frac{1}{C_e}\right)\right] \tag{20}$$

The plots of ln X vs. ε^2 at different temperatures (Fig. 9(b)) gave a linear relationship with $R^2 > 0.97$ for As(III) adsorption onto Fe-UT. The X_m and K values calculated from the slope and

Table 4
Langmuir, D–R and thermodynamics parameters for As(III) adsorption onto Fe-UT at pH 8 and different temperatures

Langmuir parameters				D–R parameters				Thermodynamics parameters		
Temperature (K)	$X_m \times 10^5$ (mol g^{-1})	K_b (L mol^{-1})	R^2	$X_m \times 10^4$ (mol g^{-1})	$K \times 10^{-9}$	E (kJ mol^{-1})	R^2	ΔG (kJ mol^{-1})	ΔH (kJ mol^{-1})	ΔS (J K^{-1} mol^{-1})
298	5.49	12,197	0.99	3.48	–5	10	0.97	–32.24		
308	5.04	9,464	0.98	3.42	–5	10	0.96	–33.34	–12	108
318	4.58	7,827	0.98	2.06	–4	11	0.92	–34.40		
328	3.91	6,980	0.97	1.34	–4	11	0.98	–35.48		

Table 5
Values of R_L for As(III) adsorption onto Fe-UT at pH 8 and different temperatures

Concentration × 10^5 (mol L^{-1})	R_L			
	Temperature (K)			
	298	308	318	328
1.40	0.85	0.88	0.90	0.91
13.1	0.38	0.44	0.49	0.52
33.4	0.19	0.24	0.27	0.30
41.1	0.16	0.20	0.23	0.25

intercept of the plots are given in Table 4. The adsorption energy was calculated from the following mathematical expression:

$$E = \frac{1}{\sqrt{-2K}} \tag{21}$$

The values of the adsorption energy (E) in the range 8–16 kJ mol^{-1} indicate chemisorption (ion exchange mechanism) while E values below 8 kJ mol^{-1} represent physisorption [2]. In the present study, adsorption energy was found to be 10 kJ mol^{-1}, which indicates that anion exchange mechanism is responsible for the adsorption of arsenite onto the surface of Fe-UT.

3.6. Comparison of adsorption capacity

The direct comparison of the adsorption capacity of Fe-UT with other adsorbents is challenging due to differences in experimental conditions which are considerably counted for the variation of the adsorption capacities. However, for the sake of comparison, the values of maximum adsorption capacity (X_m) collected from the literature for various adsorbents under the same conditions and the one observed for the iron impregnated used tea in the present study are considered. The comparison of adsorption capacity indicates that the adsorption capacity (3.34 mg g^{-1}) of Fe-UT is greater in magnitude than the adsorbents previously studied [5,14,51–53]. Hence, Fe-UT is a promising material for the removal of As(III) under the prescribed conditions as compared with other adsorbents.

3.7. Thermodynamic parameters

The changes in enthalpy (ΔH), entropy (ΔS) and Gibbs free energy (ΔG) for the adsorption of As(III) on Fe-UT at different temperatures were determined using the following equations:

$$\ln K_c = -\frac{\Delta \mathrm{H}}{RT} + \frac{\Delta \mathrm{S}}{R} \tag{22}$$

$$\Delta G = \Delta H - T\Delta S \tag{23}$$

where K_c is the equilibrium constant. The ΔH and ΔS values were calculated from the slope and intercept, respectively, of the plot of ln K_c vs. T^{-1} (Fig. 9(c)) and are given in Table 4.

The negative ΔH value suggested the exothermic nature of the adsorption process as reported by Kundu and Gupta [45] for iron oxide coated cement. As can be seen from Table 3, the decrease in ΔG value with rise of temperature shows that the feasibility of adsorption decreases with the rise of temperature, which confirms the exothermic nature of the adsorption process [45]. The negative ΔG and positive ΔS values confirm the feasibility and spontaneity of the adsorption process. Furthermore, the positive ΔS value showed increasing randomness during the adsorption of As(III) on Fe-UT and also reflected the randomness at the solid/liquid interface during arsenite adsorption onto Fe-UT.

4. Conclusions

From the overall discussion, it is concluded that UT proved to be an inefficient adsorbent for the removal of arsenite from aqueous solutions. The impregnation of the UT by iron oxide resulted in an increase in the adsorption capacity of the resultant Fe-UT. The adsorption capacity of Fe-UT was almost three times of UT. The slight release of iron in the pH range 2–3 and 10–12 indicated that the arsenite anion is dragging iron from the Fe-UT to form complexes in the aqueous phase. Maximum adsorption of As(III) in the pH range 7–8 may be correlated with the stability of Fe-UT as no release of iron from Fe-UT was observed in this pH range. In the present study, adsorption energy was found to be 10 kJ mol^{-1}, which indicates that anion exchange mechanism is responsible for the adsorption of arsenite onto the surface of Fe-UT. Thermodynamics studies showed that the adsorption of As(III) onto Fe-UT is exothermic and spontaneous in nature. Hence the present study demonstrated that Fe-UT is a viable material for the treatment of arsenic containing aqueous solution.

Acknowledgments

Authors are gratified to acknowledge the help and support provided by the National Centre of Excellence in Physical Chemistry, University of Peshawar, Pakistan for completing the research project.

References

[1] R. Ebrahimi, A. Maleki, B. Shahmoradi, H. Daraei, A.H. Mahvi, A.H. Barati, A. Eslami, Elimination of arsenic contamination from water using chemically modified wheat straw, Desal. Wat. Treat., 51 (2013) 2306–2316.
[2] M. Abid, N.K. Niazi, I. Bibi, G. Murtaza, A. Kunhikrishnan, B. Seshadri, M. Shahid, S. Ali, N.S Bolan, Y.S. Ok, F. Ali, A. Shafaqat, D.A. Igalavithana, M. Arshad, As(V) biosorption by charred orange peel in aqueous environments, Int. J. Phytorem., 18 (2016) 442–449.
[3] D. Afzali, M. Rouhani, F. Fathirad, A. Mostafavi, Selective extraction and preconcentration of ultratrace amounts of As(V) ions using carbon nanotubes as a novel sorbent, Int. J. Environ. Anal. Chem., 94 (2014) 1452–1462.
[4] L.K.D. Oliveira, C.A. Melo, D. Goveia, F.A. Lobo, L.F. Fraceto, A.H. Rosa, Adsorption/desorption of arsenic by tropical peat: influence of organic matter, iron and aluminium, Environ. Technol., 36 (2015) 149–159.
[5] D. Afzali, M. Rouhani, F. Fathirad, T. Shamspur, A. Mostafavi, Nano-iron oxide coated on sand as a new sorbent for removal of arsenic from drinking water, Desal. Wat. Treat., 57 (2016) 13030–13037.

[6] K. Babaeivelni, A.P. Khodadoust, Removal of arsenic from water using manganese (III) oxide: adsorption of As(III) and As(V), J. Environ. Sci. Health, Part A, 51 (2016) 277–288.
[7] R. Ansari, M. Sadegh, Application of activated carbon for removal of arsenic ions from aqueous solutions, E-J. Chem., 4 (2007) 103–108.
[8] S. Bibi, A. Farooqi, A. Yasmeen, M.A. Kamran, N.K. Niazi, Arsenic and fluoride removal by potato peel and rice husk ash in aqueous environments, Int. J. Phytorem., 19 (2017) 1029–1036.
[9] S.B. Gautam, R.C. Vaishya, G.L. Devnani, A.K. Mathur, Adsorption of As(III) from aqueous solutions by iron-impregnated quartz, lignite, and silica sand: kinetic study and equilibrium isotherm analysis, Desal. Wat. Treat., 52 (2014) 3178–3190.
[10] S. Sharma, K. Balasubramanian, R. Arora, Adsorption of As(v) ions onto cellulosic-ferric oxide system: kinetics and isotherm studies, Desal. Wat. Treat., 57 (2016) 9420–9436.
[11] A.L. Nashine, A.R. Tembhurkar, Batch studies of adsorptive removal of arsenite from water using coconut (*Cocos Nucifera* L.) fiber, Int. Res. J. Eng. Technol., 3 (2016) 890–894.
[12] X. Li, J. Qi, R. Jiang, J. Li, Adsorptive removal of As(III) from aqueous solution by waste litchi pericarps, Water Sci. Technol., 74 (2016) 2135–2144.
[13] S. Irem, E. Islam, Q.M. Khan, M.A.U. Haq, A.J. Hashmat, Adsorption of arsenic from drinking water using natural orange waste: kinetics and fluidized bed column studies, Water Sci. Technol. Water Supply, 17 (2017) 1149–1159.
[14] K.D. Brahman, T.G. Kazi, J.A. Baig, H.I. Afridi, S.S. Arain, S. Saraj, M.B. Arain, S.A. Arain, Biosorptive removal of inorganic arsenic species and fluoride from aqueous medium by the stem of *Tecomella undulate*, Chemosphere, 150 (2016) 320–328.
[15] F. Beduk, Superparamagnetic nanomaterial Fe_3O_4-TiO_2 for the removal of As(v) and As(III) from aqueous solutions, Environ. Technol., 37 (2016) 1790–1801.
[16] L. Dong, W. Liu, R. Jiang, Z. Wang, Study on the adsorption mechanism of activated carbon removing low concentrations of heavy metals, Desal. Wat. Treat., 57 (2016) 7812–7822.
[17] M. Faalzadeh, H. Faghihian, Separation of arsenic from aqueous solutions by amino-functionalized γ-Fe_2O_3-β-zeolite, Sep. Sci. Technol., 50 (2015) 958–964.
[18] A.K. Meher, S. Das, S. Rayalu, A. Bansiwal, Enhanced arsenic removal from drinking water by iron-enriched aluminosilicate adsorbent prepared from fly ash, Desal. Wat. Treat., 57 (2016) 20944–20956.
[19] M.B. Shakoor, N.K. Niazi, I. Bibi, G. Murtaza, A. Kunhikrishnan, B. Seshadri, M. Shahid, S. Ali, N.S. Bolan, Y.S. Ok, M. Abid, F. Ali, Remediation of arsenic-contaminated water using agricultural wastes as biosorbents, Crit. Rev. Environ. Sci. Technol., 46 (2016) 467–499.
[20] J.S. Yamani, A.W. Lounsbury, J.B. Zimmerman, Towards a selective adsorbent for arsenate and selenite in the presence of phosphate: assessment of adsorption efficiency, mechanism, and binary separation factors of the chitosan-copper complex, Water Res., 88 (2016) 889–896.
[21] M. Nandal, R. Hooda, G. Dhania, Tea wastes as a sorbent for removal of heavy metals from waste water, Int. J. Curr. Eng. Technol., 4 (2014) 243–247.
[22] H.D. Utomo, K.A Hunter, Adsorption of divalent copper, zinc, cadmium and lead ions from aqueous solution by waste tea and coffee adsorbents, Environ. Technol., 27 (2006) 25–32.
[23] E. Heraldy, R.R. Osa, V. Suryanti, Adsorption of Procion red MX 8B using spent tea leaves as adsorbent, AIP Conference Proceedings, 1710, 030025 (2016); doi: 10.1063/1.4941491.
[24] K. Bhavsar, P. Patel, Efficiency evaluation of tea waste for adsorption of hexavalent chromium from industrial effluent, Int. J. Sci. Res., 3 (2014) 229–231.
[25] M.N. Amin, Removal of As(III) from aqueous solutions by used black tea leaves, Dhaka Univ. J. Sci., 58 (2010) 275–278.
[26] A. Zuorro, R. Lavecchia, F. Medici, L. Piga, Spent tea leaves as a potential low-cost adsorbent for the removal of azo dyes from wastewater, Chem. Eng. Trans., 32 (2013) 19–24.
[27] I. Hossain, N. Anjum, T. Tasnim, Removal of arsenic from contaminated water utilizing tea waste, Int. J. Environ. Sci. Technol., 13 (2016) 843–848.
[28] D. Dickson, G. Liu, Y. Cai, Adsorption, kinetics and isotherms of arsenite and arsenate on hematite nanoparticles and aggregates, J. Environ. Manage., 186 (2017) 261–267.
[29] B.E.M. Cordero, P.A. Madrid, C.C.L. Porras, P.P. Ruiz, M.M. Yoshida, Study of the adsorption of arsenic (III and V) by magnetite nanoparticles synthesized via AACVD, Mater. Res., 19 (2016) 103–112. doi.org/10.1590/1980-5373-mr-2015-0667.
[30] P. Panneerselvam, N. Morad, K.A Tan, Magnetic nanoparticle (Fe_3O_4) impregnated onto tea waste for the removal of Ni(II) from aqueous solution, J. Hazard. Mater., 186 (2011) 160–168.
[31] V. Fristak, B.M. Richveisova, E. Viglasova, L.D. Uriska, M. Galambos, E.M. Jimenez, M. Pipiska, G. Soja, Sorption separation of Eu and As from single-component systems by Fe-modified biochar: kinetic and equilibrium study, J. Iran. Chem. Soc., 14 (2017) 521–530.
[32] X. Liu, H. Ao, X. Xiong, J. Xiao, J. Liu, Arsenic removal from water by iron-modified bamboo charcoal, Water Air Soil Pollut., 223 (2012) 1033–1044.
[33] B. Te, B. Wichitsathian, C. Yossapol, W. Wonglertarak, Development of low-cost iron mixed porous pellet adsorbent by mixture design approach and its application for arsenate and arsenite adsorption from water, Adsorption Sci. Technol., (2017) DOI: 10.1177/0263617417693626.
[34] Z. Liu, F.S. Zhang, R. Sasai, Arsenate removal from water using Fe_3O_4-loaded activated carbon prepared from waste biomass, Chem. Eng. J., 160 (2010) 57–62.
[35] F. Zhang, X. Wang, J. Xionghui, L. Ma, Efficient arsenate removal by magnetite-modified water hyacinth biochar, Environ. Pollut., 216 (2016) 575–583.
[36] O. Karaagac, H. Kockar, S. Beyaz, T. Tanrisever, A simple way to synthesize superparamagnetic iron oxide nanoparticles in air atmosphere: iron ion concentration effect, IEEE Trans. Magn., 46 (2010) 3978–3983.
[37] K. Taleb, J. Markovski, Z. Velickovic, J. Rusmirovic, M. Rancic, V. Pavlovic, A. Marinkovic, Arsenic removal by magnetite-loaded amino modified nano/microcellulose adsorbents: effect of functionalization and media size, Arab. J. Chem., (2016) DOI: 10.1016/j.arabjc.2016.08.006.
[38] T. Mahmood, R. Ali, A. Naeem, M. Hamayun, M. Aslam, Potential of used *Camellia sinensis* leaves as precursor for activated carbon preparation by chemical activation with H_3PO_4; optimization using response surface methodology, Process Saf. Environ. Prot., 109 (2017) 548–563.
[39] E. Yagmur, M. Ozmak, Z. Aktas, A novel method for production of activated carbon from waste tea by chemical activation with microwave energy, Fuel, 87 (2008) 3278–3285.
[40] T.R. Bastami, M.H. Entezari, Activated carbon from carrot dross combined with magnetite nanoparticles for the efficient removal of p-nitrophenol from aqueous solution, Chem. Eng. J., 210 (2012) 510–519.
[41] B. Liu, D. Wang, H. Li, Y. Xu, L. Zhang, As(III) removal from aqueous solution using α-Fe_2O_3 impregnated chitosan beads with As(III) as imprinted ions. Desalination, 272 (2011) 286–292.
[42] D. Ranjan, M. Talat, S. Hasan, Biosorption of arsenic from aqueous solution using agricultural residue rice polish, J. Hazard. Mater., 166 (2009) 1050–1059.
[43] T. Mahmood, S.U. Din, A. Naeem, S. Mustafa, M. Waseem, M. Hamayun, Adsorption of arsenate from aqueous solution on binary mixed oxide of iron and silicon, Chem. Eng. J., 192 (2012) 90–98.
[44] S.K. Maji, A. Pal, T. Pal, A. Adak, Adsorption thermodynamics of arsenic on laterite soil, J. Surface Sci. Technol., 22 (2007) 161–176.
[45] S. Kundu, A.K. Gupta, Adsorption characteristics of As(III) from aqueous solution on iron oxide coated cement (IOCC), J. Hazard. Mater., 142 (2007) 97–104.
[46] T.F. Lin, J.K. Wu, Adsorption of arsenite and arsenate within activated alumina grains: equilibrium and kinetics, Water Res., 35 (2001) 2049–2057.
[47] B.R.C. Vieira, A.M.A. Pintor, R.A.R. Boaventura, C.M.S. Botelho, S.C.R. Santos, Arsenic removal from water using iron-coated seaweeds, J. Environ. Manage., 192 (2017) 224–233.

[48] Z.O. Kocabas, Y. Yurum, Kinetic modeling of arsenic removal from water by ferric ion loaded red mud, Sep. Sci. Technol., 46 (2011) 2380–2390.
[49] B.S. Tawabini, S.F.A. Khaldi, M.M. Khaled, M.A. Atieh, Removal of arsenic from water by iron oxide nanoparticles impregnated on carbon nanotubes, J. Environ. Sci. Health Part A, 46 (2011) 215–223.
[50] B.K. Biswas, I. Junichi, I. Katsutoshi, G.K. Nath, H. Hiroyuki, O. Keisuke, K. Hidetaka, Adsorptive removal of As(V) and As(III) from water by a Zr(IV)-loaded orange waste gel, J. Hazard. Mater., 154 (2008) 1066–1074.
[51] V.K. Gupta, V.K. Saini, N. Jain, Adsorption of As(III) from aqueous solutions by iron oxide-coated sand, J. Colloid Interface Sci., 288 (2005) 55–60.
[52] P.K. Pandey, S. Choubey, Y. Verma, M. Pandey, K. Chandrashekhar, Biosorptive removal of arsenic from drinking water, Bioresour. Technol., 100 (2009) 634–637.
[53] B.J. Godboley, R.M. Dhoble, Removal of As(III) from groundwater by iron impregnated potato peels: batch study, Int. J. Adv. Eng. Sci. Technol., 7 (2011) 54–64.